IEEE Photonics Journal
An IEEE Photonics Society Publication

Open Access

Transmission-Efficient Structures of Bent and Crossing Silicon Slot Waveguides

Volume 5, Number 5, October 2013

Yuhei Ishizaka, Student Member, IEEE
Kunimasa Saitoh, Member, IEEE
Masanori Koshiba, Fellow, IEEE

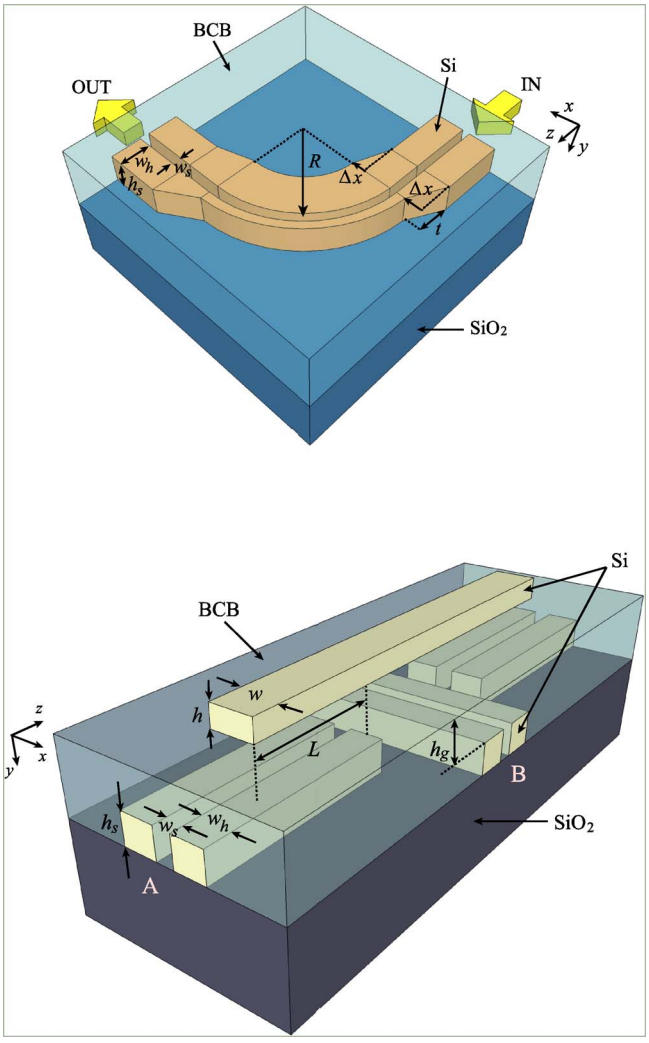

DOI: 10.1109/JPHOT.2013.2281975
1943-0655

IEEE photonics SOCIETY

IEEE

Transmission-Efficient Structures of Bent and Crossing Silicon Slot Waveguides

Yuhei Ishizaka,[1] *Student Member, IEEE*, Kunimasa Saitoh,[1] *Member, IEEE*, and Masanori Koshiba,[2] *Fellow, IEEE*

[1]Graduate School of Information Science and Technology, Hokkaido University, Sapporo 060-0814, Japan
[2]Career Center, Hokkaido University, Sapporo, Japan

DOI: 10.1109/JPHOT.2013.2281975

Manuscript received August 26, 2013; accepted September 3, 2013. Date of publication September 16, 2013; date of current version September 24, 2013. Corresponding author: Y. Ishizaka (e-mail: ishizaka@icp.ist.hokudai.ac.jp).

Abstract: We present transmission-efficient bent and crossing silicon slot waveguides for compact silicon slot waveguide-based circuits. To begin with, using the 3-D vector finite-element method, we investigate the transmission characteristics of a bent silicon slot waveguide with an asymmetric slot that is connected to straight waveguides. Numerical results show that the transmission efficiency can be improved by optimizing a taper structure that is introduced between the bend of an asymmetric slot waveguide and its straight input/output waveguides. Next, we investigate the transmission characteristics of a 3-D crossing silicon slot waveguide that has a vertical coupler. Numerical results show that our crossing structure can achieve a high transmission efficiency compared with conventional structures.

Index Terms: Slot waveguides, optical interconnects, finite-element methods.

1. Introduction

Slot waveguides can strongly confine light to the low-index sub-wavelength scale region [1], [2], which can enhance light-matter interactions. Due to the selectiveness of covered low index materials, slot waveguides are used in several applications, such as optical modulators [3], [4], optical nonlinear devices [5]–[7], biosensing circuits [8]–[10], and athermal waveguides [11], [12]. To efficiently integrate these devices, transmission-efficient bent slot waveguides and crossing slot waveguides need to be developed. Anderson *et al.* improved bending efficiency using asymmetric slot-based structures, but did not consider losses due to transitions from a straight waveguide to a bent slot waveguide [13]. Ma *et al.* presented right-angle bends based on a corner mirror and different resonant cavities, but their numerical results were limited to two-dimensional (2-D) analysis [14]. Su *et al.* proposed a design method for transmission-efficient 2-D crossing slot waveguides [15]. In [15], by filling up slots around the crossing, the transmission efficiency was improved compared with that of direct crossings. The numerical results of Su *et al.* were obtained by 2-D simulations based on the finite-difference time-domain (FDTD) method, which assumes infinite core height. In our previous work, we revealed that when considering the core height of the crossing slot waveguide in [15], a finite height caused a large coupling loss between an air slot and a Si-filled region due to the mode field mismatch [16].

In this paper, we present a transmission-efficient bent silicon slot waveguide and crossing silicon slot waveguide. To evaluate the transmission efficiency, we use the three-dimensional (3-D) vector finite-element method (VFEM) for the waveguide discontinuity problem [16]. First, we investigate the transmission characteristics of a bent silicon slot waveguide that has straight input and output

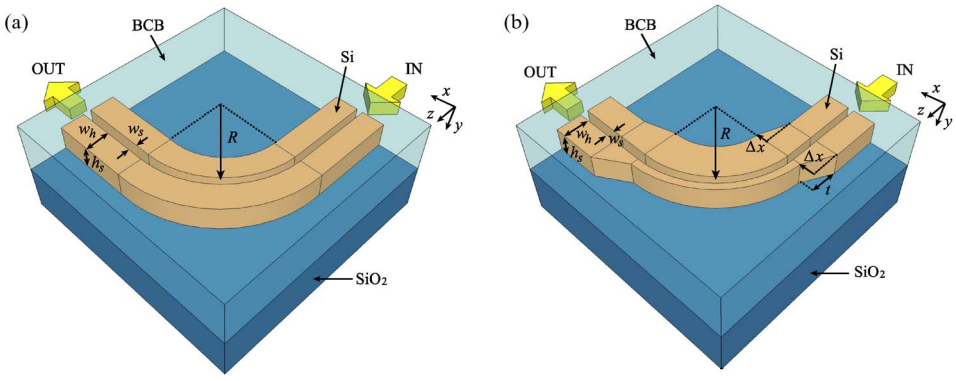

Fig. 1. Schematics of (a) a conventional silicon slot waveguide bend and (b) a silicon slot waveguide bend with an asymmetric slot.

waveguides. To construct the bent waveguide, an asymmetric geometry is employed [13]. We introduce a taper to efficiently connect the bent region to the straight waveguides. Numerical results show that the transmission efficiency is increased by optimizing parameters of the taper geometry. When the bending radius is 1 μm, the transmission efficiency is greatly improved from 33.8% to 84.2%. Next, we investigate the transmission characteristics of a 3-D crossing slot waveguide that has a vertical coupler. A comparison between the proposed structure and the conventional crossing structure [16] shows that the maximum transmission efficiency increases from 78.2% to 95.9%.

2. Bent Silicon Slot Waveguides

Fig. 1(a) and (b) shows schematics of a conventional silicon slot waveguide bend and a silicon slot waveguide bend that has an asymmetric slot, respectively. Typically, the slot region is filled with certain materials, for example, electro-optic material [3], nonlinear material [5], aqueous solution [8], and materials for athermal waveguides [11], [12]. In our work, the silicon slot waveguide is embedded with benzocyclobutene (BCB), which can be used for athermal on-chip interconnects [11]. We assume that the refractive indexes of Si, SiO_2, and BCB are 3.47, 1.45, and 1.54, respectively. In the structure, the length of the straight input/output waveguide is 2 μm. We define the slot width, the waveguide height, and the Si-width as w_s, h, and w_h, respectively. The bending radius is defined as R. In addition, we define the taper length and the offset distance as t and Δx, respectively.

To investigate the influence of the parameter selection, we evaluated the effective refractive index n_{eff}, bending loss, and the confinement factor when changing slot width and waveguide height. Fig. 2(a) and (b) shows the effective refractive index and the bending loss of the silicon slot waveguide as a function of w_h, respectively. We can see that the effective refractive index increases as w_h becomes larger. From Fig. 2(a) and (b), we can see that the bending loss is related to the effective refractive index. Specifically, it has been noted that a high effective refractive index leads to reduction of the bending loss. Fig. 2(c) shows the confinement factor in the cover medium (slot region) when changing w_h. The confinement factor Γ is evaluated using the following equation [17]:

$$\Gamma = \frac{\iint_{\text{slot}} \text{Re}(\boldsymbol{E} \times \boldsymbol{H}^*) \cdot i_z dxdy}{\iint_{\text{total}} \text{Re}(\boldsymbol{E} \times \boldsymbol{H}^*) \cdot i_z dxdy} \tag{1}$$

where $\boldsymbol{E}$ and $\boldsymbol{H}$ are the electric field and the magnetic field, respectively, and $*$ denotes the complex conjugate. If we choose parameters that result in a high effective refractive index, we can obtain a low bending loss. However, the effect of the slot waveguide, namely, the contribution of

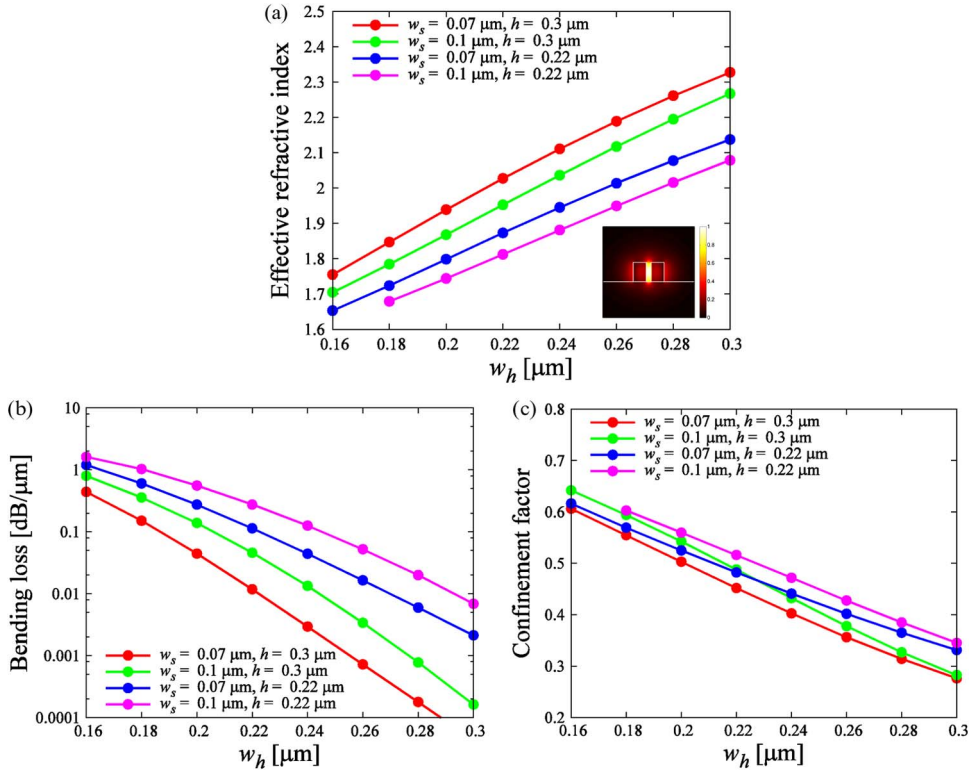

Fig. 2. (a) The effective refractive index, (b) the bending loss, and (c) the confinement factor of the silicon slot waveguide as a function of the Si-width w_h.

the strong light confinement in the slot region, becomes weaker if the confinement factor is small. In other words, there exists a trade-off between the bending loss and the effect of the light confinement in the slot region. Here, we set the slot width of 0.07 μm and the waveguide height of 0.3 μm, which have been used for the conventional slot waveguides [15], [16]. Then, considering the trade-off relation, we set w_h to 0.2 μm ($n_{eff} = 1.939$) for the bent silicon slot waveguide. Indeed, several studies set the effective refractive index of less than 2.0 [12], [18].

To investigate the influence of the coupling loss between a bent region and straight waveguides, we evaluated the transmission characteristics of the bent silicon slot waveguide having straight input/output ports [Fig. 1(a)] and a uniform 90-degree bend without straight input/output ports, as shown in Fig. 3(b). In the 3-D simulation, the normalized transmission power P is obtained by the mode overlap integral:

$$P = \left| \frac{\iint (\boldsymbol{E}_{out} \times \boldsymbol{H}_0^*) \cdot i_z dzdy}{\iint (\boldsymbol{E}_{in} \times \boldsymbol{H}_{in}^*) \cdot i_x dxdy} \right|^2, \tag{2}$$

where $\boldsymbol{E}_{in}$ and $\boldsymbol{H}_{in}$ are the electric field and the magnetic field at the input port, respectively. $\boldsymbol{E}_{out}$ and $\boldsymbol{H}_0$ are the propagated electric field and the intrinsic magnetic field at the output port, respectively. On the other hand, the transmission efficiency of the uniform 90-degree bend [Fig. 3(a)] is evaluated using the cylindrical coordinate based 2-D VFEM [19], from which the bending loss [dB/μm] is obtained. The transmission efficiency $P_{uniform}$ of the uniform 90-degree bend is calculated using the following equation:

$$10\log P_{uniform} = (Bending\ loss[\mathrm{dB}/\mu\mathrm{m}])\frac{\pi R}{2}. \tag{3}$$

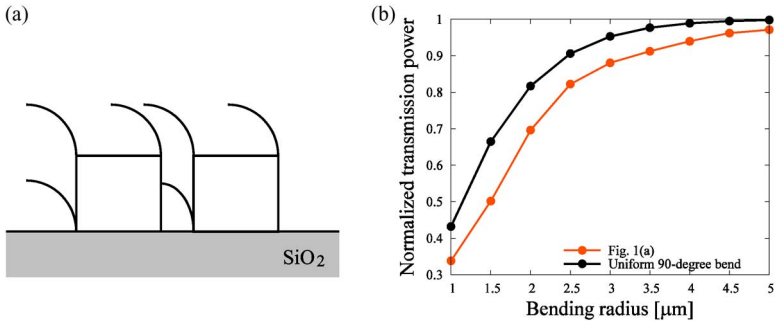

Fig. 3. (a) Schematic of a uniform 90-degree bend of the silicon slot waveguide without straight input/output ports, and (b) the transmission characteristics of the bent silicon slot waveguide with straight input/output ports [Fig. 1(a)] and the uniform 90-degree bend.

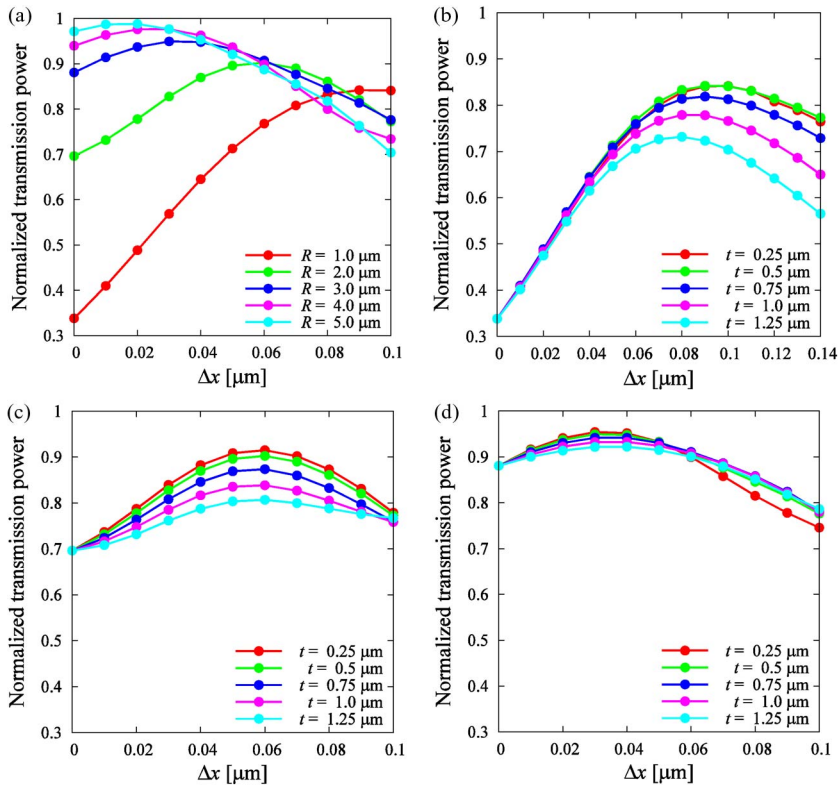

Fig. 4. (a) The transmission efficiency with respect to Δx when $t = 0.5$ μm, and the transmission efficiency as functions of Δx and t when (b) $R = 1$ μm, (c) $R = 2$ μm, and (d) $R = 3$ μm.

In Fig. 3(b), the difference of transmission efficiency at the same bending radius corresponds to the coupling loss between the bent region and the straight input and output waveguides. When $R = 5$ μm and $R = 2$ μm, the coupling losses are 0.11 dB and 0.69 dB, respectively.

We consider the silicon slot waveguide bend with an asymmetric slot [Fig. 1(b)]. We introduce a taper to connect the asymmetric slot bend to the straight input/output waveguides. At the junction points, the slot geometry is not changed, while the outer geometry near the cladding is transformed because the light intensity in the cladding is weaker than that in the slot. Fig. 4(a) shows the transmission efficiency with respect to Δx when $t = 0.5$ μm. Results of the normalized transmission power at $\Delta x = 0$ μm correspond to the case of the conventional silicon slot waveguide bend. We

TABLE 1
Comparison between the conventional bent structure and our bent structure when $t = 0.5$ μm

R [μm]	Transmission efficiency for Fig. 1(a) [%]	Maximum transmission efficiency for Fig. 1(b) [%]
1	33.8	84.2
2	69.6	90.2
3	88.0	94.9
4	93.9	97.6
5	97.1	98.7

can see that the transmission efficiency at each bending radius is improved by optimizing Δx. Compared with the conventional silicon slot waveguide bend $(\Delta x = 0)$, the transmission efficiency increases from 88.0% to 94.9% when $R = 3$ μm and from 97.1% to 98.7% when $R = 5$ μm. When $R = 1$ μm, the transmission efficiency is drastically improved from 33.8% to 84.2%. We can see that the improvement of the transmission efficiency becomes larger as the bending radius decreases. The offset distance that results in the maximum transmission efficiency also becomes larger as the bending radius decreases. These comparisons are summarized in Table 1. To optimize the taper geometry, we evaluated the normalized transmission power as functions of the taper length t and the offset distance Δx, as shown in Fig. 4(b)–(d). In the case of $R = 1$ μm and $R = 2$ μm, the transmission is improved as the taper length becomes shorter. On the other hand, when $R = 3$ μm, the transmission is slightly improved as the taper length becomes shorter. In other words, the influence of the taper length is low when the bending radius is large. Compared with the right-angle slot waveguide bend whose maximum transmission was 94.3% [14] (state-of-the-art), our bent structure can achieve a high transmission when $R > 3$ μm.

We estimate the propagation loss of our proposed bent structure. According to [20], the measured propagation loss of the silicon slot waveguide that has $w_s = 0.1$ μm, $h = 0.22$ μm, and $w_h = 0.27$ μm was 16.7 dB/cm. After conducting five cycles of the RCA clean, the propagation loss of the silicon slot waveguide was reduced from 16.7 dB/cm to 7.0 dB/cm for the quasi-TE mode [20]. The propagation loss for the mode is approximately given by the product of the confinement factor and the scattering attenuation coefficient in the sidewalls [20]. The confinement factor of the reported silicon slot waveguide is 0.4, as shown Fig. 2(c). Therefore, the propagation loss of our structure is estimated to be about 25% larger than the reported silicon slot waveguide because the confinement factor of our structure is 0.5.

3. Crossing Silicon Slot Waveguides

A method for designing efficiently transmitting crossing silicon slot waveguides was proposed [15]. By filling up the slots around the cross, the transmission was improved compared with conventional direct crossings. However, their numerical results were obtained by 2-D simulations based on the FDTD method. Therefore, in our previous work, we investigated the transmission characteristics of a crossing silicon slot waveguide with finite core height and revealed that this crossing structure has a large coupling loss between the slot waveguide and the Si-filled segment [16].

To avoid the coupling loss due to the mode field mismatch, we propose in this article a 3-D crossing silicon slot waveguide with a vertical coupler, as shown in Fig. 5(a) and (b). The slot waveguide is embedded with BCB, and a Si wire waveguide, which is the vertical coupler, is bonded on the BCB surface. We assume that the refractive indexes of Si, SiO_2, and BCB are 3.47, 1.45, and 1.54, respectively. In the proposed structure, the slot width and height are $w_s = 0.07$ μm and $h_s = 0.3$ μm, respectively [16]. To make the coupling length as short as possible, we set w_h to 0.18 μm. The coupling length is determined by the overlap of the evanescent fields in two parallel waveguides. To obtain a large overlap of the evanescent fields, a structure that has a low effective refractive index should be selected. We define the width and height of the Si wire as w and h, respectively. The distance between the Si wire waveguide and the slot waveguide is defined as h_g,

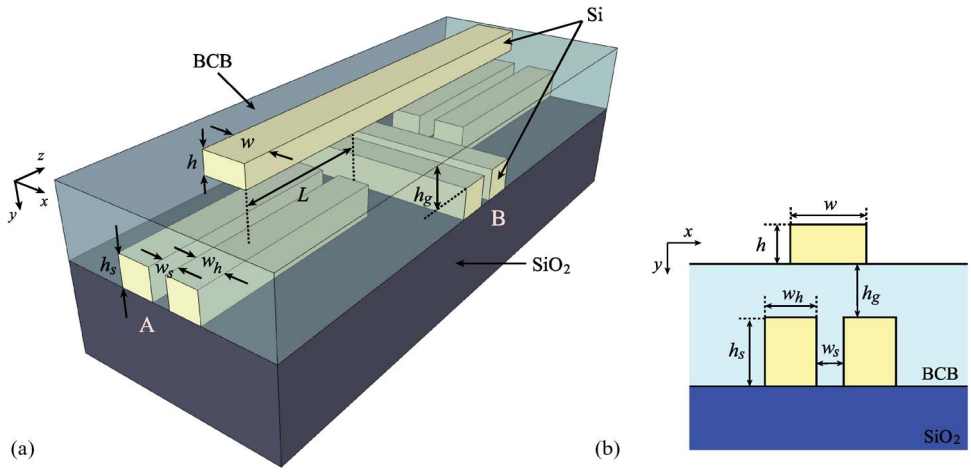

Fig. 5. Schematic of (a) a three-dimensional crossing silicon slot waveguide with a vertical coupler and (b) the $x - y$ plane in the coupling region.

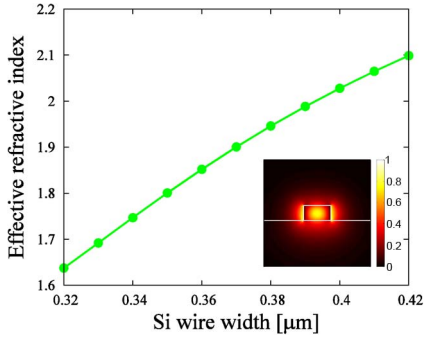

Fig. 6. The effective refractive index of the Si wire waveguide as a function of the width of the Si wire when $h = 0.2$ μm.

and the length of the parallel region is L. Our proposed crossing silicon slot waveguide can be fabricated as follows. A Si under layer is first etched to form slot waveguides, and BCB can be spin-coated on the slot waveguides [11]. Next, a Si wire waveguide can be bonded on the BCB surface [21]. Another possible fabrication way is to deposit amorphous silicon. After embedding BCB, amorphous silicon can be deposited on the BCB surface [22]. And then, the amorphous silicon layer can be etched to form a Si wire waveguide. Fig. 6 shows the effective refractive index of the Si wire waveguide as a function of the width of the Si wire when $h = 0.2$ μm. To achieve the phase matching between modes of the slot waveguide and the Si wire, we set the width of the Si wire to 0.36 μm because the effective refractive index of the slot waveguide is 1.847 [Fig. 2(a)]. To determine a value of L, we conducted an eigen mode analysis for an $x - y$ plane in the coupling region [Fig. 5(b)]. Using the obtained effective refractive indexes of supermodes, we can calculate the coupling length L_c as follows:

$$L_c = \frac{\lambda}{2(n_{eff,0} - n_{eff,1})}, \tag{4}$$

where $n_{eff,0}$ and $n_{eff,1}$ are the effective refractive indexes of the fundamental supermode and the first order supermode, respectively, and λ is the operating wavelength. From Eq. (4), L_c becomes 6.25 μm when $h_g = 0.35$ μm.

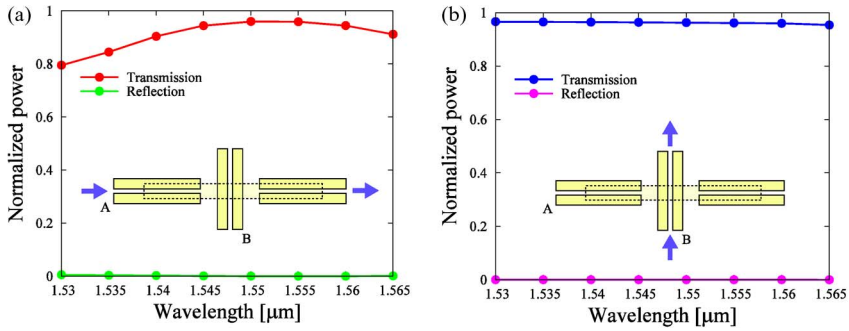

Fig. 7. The wavelength dependence of the normalized transmission and reflection powers when light is inputted from (a) port A and (b) port B.

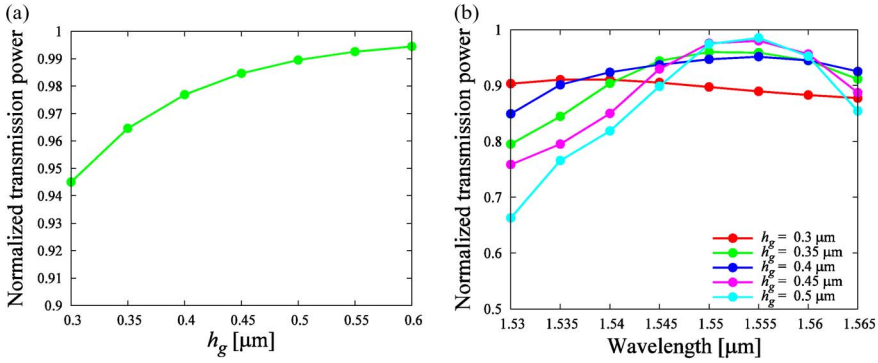

Fig. 8. (a) The normalized transmission power as a function of h_g when light is inputted from port B, and (b) the wavelength dependence of the normalized transmission power with respect to h_g when light is inputted from port A.

First, we set L to 6.25 μm and h_g to 0.35 μm. Fig. 7(a) shows the wavelength dependence of the normalized transmission and reflection powers when light is inputted from port A. We find that the transmission efficiency is over 79.5% in the whole C-band, whereas the normalized reflection is less than 0.5% in the whole C-band. Typically, the crosstalk in a 3-D crossing waveguide is smaller than the back reflection [23]. Our structure can also achieve this condition. The maximum transmission efficiency increases from 78.2% for the conventional crossing structure [16] to 95.9% for our proposed structure. Fig. 7(b) shows the wavelength dependence of the normalized transmission and reflection powers when light is inputted from port B. We find that the transmission efficiency is over 95.3% in the whole C-band. However, the transmission efficiency when light is inputted from port B is somewhat low, even though light is not coupled into the Si wire waveguide. To understand this result, we evaluated the transmission efficiency with respect to h_g. Fig. 8(a) shows the normalized transmission power as a function of h_g when light is inputted from port B. From this figure, we can see that the transmission efficiency exceeds 99% if h_g is over 0.5 μm. A possible explanation is that the scattering loss occurs due to a collision with the Si wire waveguide when h_g is small. Fig. 8(b) shows the wavelength dependence of the normalized transmission power with respect to h_g when light is inputted from port A. Here, the values of L, which is given by Eq. (4), are summarized in Table 2. When choosing a large h_g, the transmission bandwidth tends to become narrower. On the other hand, the transmission bandwidth tends to become wider when choosing a small h_g, while the maximal transmission decreases. We can conclude that there exists a trade-off between the transmission bandwidth and the highest transmission power when light is inputted from port A. Recently, a crossing slot waveguide using the slot-to-strip mode converter and the strip-multimode-waveguide

TABLE 2

The values of h_g and L

h_g [μm]	L [μm]
0.3	4.8
0.35	6.25
04	8.11
0.45	10.45
0.5	13.4

crossing has been proposed [24] (state-of-the-art). The reported structure has a large bandwidth and a high transmission of 98%, but results were obtained by the 2-D simulations. In the 3-D structure of the multimode-interference-based crossing waveguide, transmission was 95.3% at the wavelength of 1.55 μm [25]. Therefore, although the bandwidth is reduced, our crossing structure achieves a high transmission compared with the state-of-the-art [24].

4. Conclusion

We presented a transmission-efficient bent silicon slot waveguide with asymmetric geometry at the bending slot region and investigated the transmission efficiency using the 3-D VFEM. We introduced a taper to efficiently connect the asymmetric bent region to straight waveguides. Numerical results showed that the transmission efficiency is increased by optimizing parameters of the taper geometry. We found that the improvement of the transmission efficiency becomes larger as the bending radius becomes smaller. We also proposed a 3-D crossing silicon slot waveguide that has a vertical coupler and investigated its transmission efficiency using the 3-D VFEM. Numerical results showed that our crossing structure can achieve a high transmission efficiency compared with conventional structures. The presented transmission-efficient bent and crossing silicon slot waveguides will be able to promote the integration of slot waveguide-based circuits.

References

[1] V. R. Almeida, Q. Xu, C. A. Barrios, and M. Lipson, "Guiding and confining light in void nanostructure," *Opt. Lett.*, vol. 29, no. 11, pp. 1209–1211, Jun. 2004.
[2] Q. Xu, V. R. Almeida, R. Panepucci, and M. Lipson, "Experimental demonstration of guiding and confining light in nanometer-size low-refractive-index material," *Opt. Lett.*, vol. 29, no. 14, pp. 1626–1628, Jul. 2004.
[3] M. Hochberg, T. Baehr-Jones, G. Wang, J. Huang, P. Sullivan, L. Dalton, and A. Scherer, "Towards a millivolt optical modulator with nano-slot waveguides," *Opt. Exp.*, vol. 15, no. 13, pp. 8402–8410, Jun. 2007.
[4] Y. Enami, B. Yuan, M. Tanaka, J. Luo, and A. K.-Y. Jen, "Electro-opticpolymer/TiO_2 multilayer slot waveguide modulators," *Appl. Phys. Lett.*, vol. 101, no. 12, pp. 123509-1–123509-4, Sep. 2012.
[5] T. Vallaitis, S. Bogatscher, L. Alloatti, P. Dumon, R. Baets, M. L. Scimeca, I. Biaggio, F. Diederich, C. Koos, W. Freude, and J. Leuthold, "Optical properties of highly nonlinear silicon-organic hybrid (SOH) waveguide geometries," *Opt. Exp.*, vol. 17, no. 20, pp. 17 357–17 368, Sep. 2009.
[6] A. Martínez, J. Blasco, P. Sanchis, J. V. Galán, J. García-Rupérez, E. Jordana, P. Gautier, Y. Lebour, S. Hernández, R. Spano, R. Guider, N. Daldosso, B. Garrido, J. M. Fedeli, L. Pavesi, and J. Martí, "Ultrafast all-optical switching in a silicon-nanocrystal-based silicon slot waveguide at telecom wavelength," *Nano Lett.*, vol. 10, no. 4, pp. 1506–1511, Mar. 2010.
[7] Q. Liu, S. Gao, Z. Li, Y. Xie, and S. He, "Dispersion engineering of a silicon-nanocrystal-based slot waveguide for broadband wavelength conversion," *Appl. Opt.*, vol. 50, no. 9, pp. 1260–1265, Mar. 2011.
[8] F. Dell'Olio and V. M. N. Passaro, "Optical sensing by optimized silicon slot waveguides," *Opt. Exp.*, vol. 15, no. 8, pp. 4977–4993, Apr. 2007.
[9] C. A. Barrios, K. B. Gylfason, B. Sánchez, A. Griol, H. Sohlström, M. Holgado, and R. Casquel, "Slot-waveguide biochemical sensor," *Opt. Lett.*, vol. 32, no. 21, pp. 3080–3082, Nov. 2007.
[10] Q. Liu, J. S. Kee, and M. K. Park, "A refractive index sensor design based on grating-assisted coupling between a strip waveguide and a slot waveguide," *Opt. Exp.*, vol. 21, no. 5, pp. 5897–5909, Mar. 2013.
[11] J.-M. Lee, D.-J. Kim, G.-H. Kim, O.-K. Kwon, K.-J. Kim, and G. Kim, "Controlling temperature dependence of silicon waveguide using slot structure," *Opt. Exp.*, vol. 16, no. 3, pp. 1645–1652, Feb. 2008.
[12] Y. Atsumi, K. Inoue, N. Nishiyama, and S. Arai, "Athermal wavelength characteristics of Si slot ring resonator embedded with benzocyclobutene for optoelectronic integrated circuits," *Jpn. J. Appl. Phys.*, vol. 49, no. 5, pp. 050206-1–050206-3, May 2010.

[13] R. A. Anderson, B. S. Schmidt, and M. Lipson, "High confinement in silicon slot waveguides with sharp bends," *Opt. Exp.*, vol. 14, no. 20, pp. 9197–9202, Oct. 2006.
[14] C. Ma, Q. Zhang, and E. V. Keuren, "Right-angle slot waveguide bends with high bending efficiency," *Opt. Exp.*, vol. 16, no. 19, pp. 14 330–14 334, Sep. 2008.
[15] R. Su, D. Tang, W. Ding, L. Chen, and Z. Zhou, "Efficient transmission of crossing dielectric slot waveguides," *Opt. Exp.*, vol. 19, no. 5, pp. 4756–4761, Feb. 2011.
[16] Y. Ishizaka, Y. Kawaguchi, K. Saitoh, and M. Koshiba, "Three-dimensional finite-element solutions for crossing slot-waveguides with finite core-height," *J. Lightw. Technol.*, vol. 30, no. 21, pp. 3394–3400, Nov. 2012.
[17] N.-N. Feng, J. Michel, and L. C. Kimerling, "Optical field concentration in low-index waveguide," *IEEE J. Quantum Electron.*, vol. 42, no. 9, pp. 885–890, Sep. 2006.
[18] P. Sanchis, J. Blasco, A. Martínez, and J. Martí, "Design of silicon-based slot waveguide configurations for optimum nonlinear performance," *J. Lightw. Technol.*, vol. 25, no. 5, pp. 1298–1305, May 2007.
[19] K. Kakihara, N. Kono, K. Saitoh, and M. Koshiba, "Full-vectorial finite element method in a cylindrical coordinate system for loss analysis of photonic wire bends," *Opt. Exp.*, vol. 14, no. 23, pp. 11 128–11 141, Nov. 2006.
[20] H. Sun, A. Chen, D. Abeysinghe, A. Szep, and R. S. Kim, "Reduction of scattering loss of silicon slot waveguides by RCA smoothing," *Opt. Lett.*, vol. 37, no. 1, pp. 13–15, Jan. 2012.
[21] Y. Halioua, A. Bazin, P. Monnier, T. J. Karle, G. Roelkens, I. Sagnes, R. Raj, and F. Raineri, "Hybrid III-V semiconductor/silicon nanolaser," *Opt. Exp.*, vol. 19, no. 10, pp. 9221–9231, May 2011.
[22] R. Sun, P. Dong, N. Feng, C. Hong, J. Michel, M. Lipson, and L. Kimerling, "Horizontal single and multiple slot waveguides: Optical transmission at $\lambda = 1550$ nm," *Opt. Express*, vol. 15, no. 26, pp. 17 967–17 972, Dec. 2007.
[23] A. V. Tsarev, "Efficient silicon wire waveguide crossing with negligible loss and crosstalk," *Opt. Exp.*, vol. 19, no. 15, pp. 13 732–13 737, Jul. 2011.
[24] Y. Xu, J. Wang, J. Xiao, and X. Sun, "Design of a compact silicon-based slot-waveguide crossing," *Appl. Opt.*, vol. 52, no. 16, pp. 3737–3744, Jun. 2013.
[25] C.-H. Chen and C.-H. Chiu, "Taper-integrated multimode-interference based waveguide crossing design," *IEEE J. Quantum Electron.*, vol. 46, no. 11, pp. 1656–1661, Nov. 2010.